

****FULL TITLE****
*ASP Conference Series, Vol. **VOLUME**, **YEAR OF PUBLICATION***
****NAMES OF EDITORS****

Five ideas on black hole accretion disks

Marek A. Abramowicz

Physics Department, Göteborg University, SE-412-96 Göteborg, Sweden
Copernicus Astronomical Center, Bartycka 18, 00-716 Warsaw, Poland

Abstract. I review five of Bohdan Paczyński’s ideas on black hole accretion disk theory. They formed my understanding of the subject and often guided intuition in my research. They are fundamentally profound, rich in physical consequences, mathematically elegant and clever, and in addition are useful in several technically difficult practical applications.

1. Introduction

1.1. Motivation: the five “easy” pieces

This review article does not give a full (or even coherent) description of black hole accretion disk theory. Instead, it only reflects briefly on a few of Bohdan Paczyński’s particularly important contributions to the subject. Bohdan had several brilliant ideas about black hole accretion. Today, most of them are mainstream and firmly accepted. One is still considered controversial.

1. *The Potential:* For free particles, both Newton’s and Einstein’s orbital dynamics are described by the same principle, and indeed the same equation: the orbital frequency follows from the first derivative, and the epicyclic frequencies follow from the second derivatives of the “effective potential”. Therefore, as Bohdan pointed out, by a proper definition of an artificial Newtonian potential, one should be able to accurately describe (formally in Newton’s theory!) the fully general relativistic orbital motion. He then guessed the form of the “Paczyński-Wiita” potential which immediately became a great success. The potential is simple and very practical in numerous applications.

2. *The Doughnut:* One is often interested in phenomena that occur on a “dynamical” timescale t_* much shorter than the “viscous” time $t_{\mathcal{L}}$ needed for angular momentum redistribution, and the “thermal” time $t_{\mathcal{S}}$ needed for entropy redistribution. In modeling such cases, Bohdan noticed, the angular momentum and entropy distributions may be considered *free functions*. Therefore, when studying processes with $t_* \ll t_0 = \text{Min}(t_{\mathcal{L}}, t_{\mathcal{S}})$, one may ad hoc *assume* angular momentum and entropy distributions. A constant angular momentum is the simplest possible assumption. It was used by Bohdan and his Warsaw team to construct the “Polish Doughnuts”, i.e. super-Eddington thick accretion disks.

3. *The Funnel:* In Warsaw we found that a long, narrow empty funnel forms along the axis of rotation of a Polish doughnut. It collimates radiation to hyper-Eddington fluxes.

4. *The Roche Lobe:* In equilibrium, the isobaric surfaces of the accretion disk coincide with the surfaces of constant effective potential, called the “equipo-

tential” surfaces. Near a black hole one of the equipotential surfaces, called the “Roche lobe”, self-crosses along the “cusp”, i.e. a circle $r = r_{cusp}$ located between the innermost stable circular orbit at $r = r_{ISCO}$, and the marginally bound orbit at $r = r_{mb}$. Bohdan’s knowledge of close binaries helped him to realize that the black hole Roche lobe overflow must induce dynamical mass loss from the disk. Thus, for $r < r_{cusp}$ accretion is not caused by “stresses” that remove angular momentum, but by the strong gravity. The “inner edge” of an accretion disk is at the ISCO only for accretion flows with very small \dot{M}/\dot{M}_{Edd} that are radiatively efficient (Shakura-Sunyaev). He understood that the efficiency of accretion η (defined by $L = \eta \dot{M} c^2$) equals the Keplerian binding energy at the location of the cusp: when $r_{cusp} = r_{ISCO}$, efficiency takes its maximal possible value, but it goes to zero when r_{cusp} approaches r_{mb} . All radiatively inefficient accretion flows (RIAFs) like advection-dominated accretion flows (adafs) and slim disks have their inner edges close to r_{mb} .

5. *The Inner Torque:* Against the view of an influential part of the black hole community, Bohdan argued that when the accretion disk is vertically very thin, for very small accretion rates the viscous or magnetohydrodynamic (MHD) torque at the inner edge should be vanishingly small.

1.2. Analytic models and computer simulations

Bohdan was a master of massive supercomputing methods in astrophysics. Some of the computer codes that he developed, e.g. for stellar structure and evolution, are the standard tools in the field. However, although supercomputer MHD simulations are a large part of black hole accretion research today, Bohdan was not himself involved in this activity. Indeed, all Bohdan’s ideas that I discuss here are based on simple analytic models. One may ask — why? This I do not know, but I can think of a possible reason. The present-day MHD simulations do not address the fundamental problems that the theory of black hole accretion faces. Our understanding of black hole accretion rests on analytic models. Indeed, all the fundamental features of black hole accretion flows that have been calculated in MHD simulations, were *previously well understood* in terms of analytic models. It seems that today, and in the foreseeable future, the super-computer simulations will keep confirming rather than solving or discovering. Today, the most important message of the supercomputer simulations seems to be that the approximations and simplifications adopted in the analytic models have been rather wisely chosen (see Figure 1 to illustrate this point).

1.3. Notation and units

In this review, I use the Kerr metric in the standard spherical Boyer-Lindquist coordinates t, ϕ, r, θ with the $+- --$ signature. The Kerr metric is stationary and axially symmetric,

$$ds^2 = g_{tt} dt^2 + 2g_{t\phi} dt d\phi + g_{\phi\phi} d\phi^2 + g_{rr} dr^2 + g_{\theta\theta} d\theta^2, \quad (1)$$

i.e. its metric tensor components are (known) functions of radial and polar coordinates r, θ , the mass M and the dimensionless spin parameter $|a| < 1$,

$$g_{ik} = g_{ik}(r, \theta; M, a). \quad (2)$$

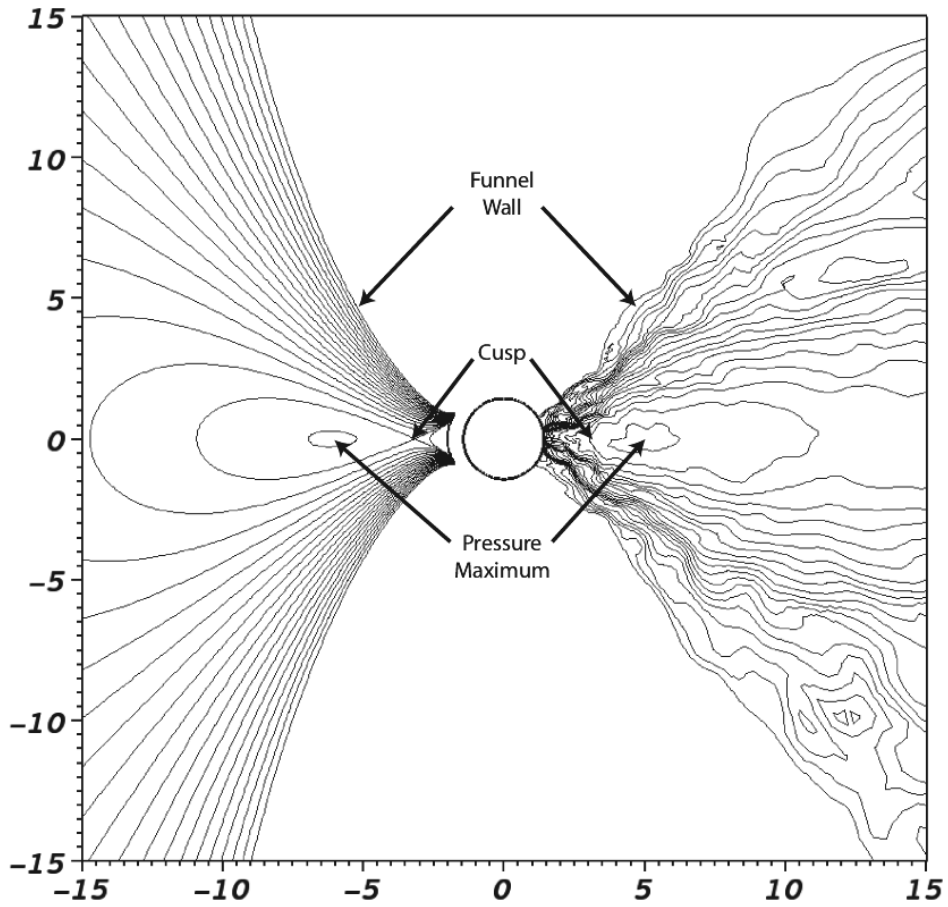


Figure 1. Isobaric surfaces in a black hole accretion flow. Left: according to a very simple, analytic Polish doughnut model. Right: according to a state-of-art, full 3D MHD numerical simulation. Figure taken from the *Living Review on black hole accretion disks* by Abramowicz & Fragile, in preparation.

However, in all specific examples, I will use a much simpler Schwarzschild metric that describes spacetime geometry of a non-rotating ($a = 0$) black hole,

$$ds^2 = \left(1 - \frac{r_G}{r}\right) dt^2 - \left(1 - \frac{r_G}{r}\right)^{-1} dr^2 - r^2 [d\theta^2 + \sin^2 \theta d\phi^2], \quad (3)$$

with the gravitational radius r_G is defined by,

$$r_G \equiv \frac{2GM}{c^2} \quad (4)$$

My apologies to Bohdan; here I often but not always use the $c = 1 = G$ units he greatly disliked.

2. The Potential

According to Newton's theory of gravity, the motion of a free particle in a stationary, axially symmetric gravitational potential $\Phi(r, \theta)$, is confined to a plane, which may be chosen as the "equatorial plane", $\theta = \pi/2$. Circular orbits in the equatorial plane are characterized by

$$r = r_0 = \text{const}, \quad \theta = \theta_0 = \frac{\pi}{2} = \text{const}, \quad (5)$$

and the slightly non-circular, slightly off-plane orbits are characterized by

$$\delta r(t) \equiv r(t) - r_0 \ll r_0, \quad \delta \theta(t) \equiv \theta(t) - \theta_0 \ll \theta_0. \quad (6)$$

The specific (per unit mass) energy $\mathcal{E} = [V^2 + (v_\phi)^2]/2 + \Phi$ and the specific angular momentum $\mathcal{L} = r v_\phi$ are constants of motion. Here $V^2 = (v_r)^2 + (v_\theta)^2 \equiv (\delta \dot{r})^2 + (\delta \dot{\theta})^2 \ll (v_\phi)^2$. One defines the effective potential

$$\mathcal{U}(r, \theta, \mathcal{L}) = \Phi(r, \theta) + \frac{\mathcal{L}^2}{2r^2 \sin^2 \theta}, \quad (7)$$

and writes,

$$\frac{1}{2}V^2 = \mathcal{E} - \mathcal{U}(r, \theta, \mathcal{L}). \quad (8)$$

The Keplerian angular momentum distribution $\mathcal{L} = \mathcal{L}_K(r)$ in strictly circular orbits (5) follows from the condition,

$$\left(\frac{\partial \mathcal{U}}{\partial r}\right)_{\mathcal{L}} = 0, \quad (9)$$

while the deviations (6) obey the simple harmonic oscillator equation¹

$$\delta \ddot{r} + \omega_r^2 \delta r = 0, \quad \delta \ddot{\theta} + \omega_\theta^2 \delta \theta = 0, \quad (10)$$

¹When deriving the "radial" equation, one puts $V = dr/dt = \delta \dot{r}$ in (8), and when deriving the "vertical" equation one puts $V = d\theta/dt = \delta \dot{\theta}$ in (8).

with the “radial” ω_r , and the “vertical” ω_θ epicyclic frequencies given by,

$$\omega_r^2 = \left(\frac{\partial^2 \mathcal{U}}{\partial r^2} \right)_{\mathcal{L}}, \quad \omega_\theta^2 = \left(\frac{\partial^2 \mathcal{U}}{\partial \theta^2} \right)_{\mathcal{L}}. \quad (11)$$

So much for the Newtonian case. The fully relativistic case is remarkably similar. The relativistic analog of the Newtonian condition for strictly circular orbits (5) may be written as a condition for the components of a particle’s four-velocity $u^i = dx^i/ds$,

$$u^i = (u^t, u^\phi), \quad u^r = 0, \quad u^\theta = 0. \quad (12)$$

The nearly-circular orbits are characterized by,

$$u^i = (u^t, u^\phi, u^r, u^\theta), \quad (u^r, u^\theta) \ll (u^t, u^\phi). \quad (13)$$

As in Newton’s theory, the energy and angular momentum are two constants of the free (i.e. geodesic) motion. Their standard definitions read $\mathcal{E}^* = u_t$ $\mathcal{L}^* = -u_\phi$, but for our purpose it is convenient to rescale them according to,

$$\mathcal{E}_{\text{Kerr}} = \ln \mathcal{E}^*, \quad \mathcal{L}_{\text{Kerr}} = \frac{\mathcal{L}^*}{\mathcal{E}^*}. \quad (14)$$

Obviously, $\mathcal{E}_{\text{Kerr}}$ and $\mathcal{L}_{\text{Kerr}}$ are also constants of geodesic motion. It is also convenient to define the small “deviation” velocity V by its square,

$$V_{\text{Kerr}}^2 = 2 \ln \left[1 - g_{rr}(u^r)^2 - g_{\theta\theta}(u^\theta)^2 \right] \ll 1, \quad (15)$$

which is obviously always positive because $-g_{rr} > 0$ and $-g_{\theta\theta} > 0$. Then, most importantly, one introduces the effective potential,

$$\mathcal{U}_{\text{Kerr}} = -\frac{1}{2} \ln \left(g^{tt} - 2\mathcal{L}g^{t\phi} + \mathcal{L}^2 g^{\phi\phi} \right). \quad (16)$$

With these definitions, one may easily cast the general equation $u_i u_k g^{ik} = 1$ into the form

$$\frac{1}{2} V_{\text{Kerr}}^2 = \mathcal{E}_{\text{Kerr}} - \mathcal{U}_{\text{Kerr}}(r, \theta, \mathcal{L}_{\text{Kerr}}), \quad (17)$$

which is identical with the corresponding Newtonian equation (8). All quantities that appear in (17) have the same physical meaning as the corresponding Newtonian quantities, and go to the right limits when $v_\phi/c \ll 1$, $V/c \ll 1$, $(2GM/c^2)/r = r_G/r \ll 1$. *The same equations have the same solutions*² and therefore one may just use the same procedure as in Newton’s theory to get the Keplerian angular momentum from the first derivative of the effective potential, i.e. from equation (9), and the epicyclic frequencies from the second derivatives of the potential, i.e. from equation (11). This is indeed the standard, text-book way used in general relativity. For example, in the special case of a non-rotating

²This well-known remark by Richard Feynman is “unsourced” according to wikiquote.

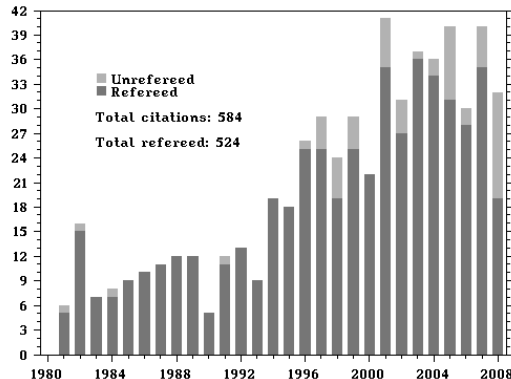


Figure 2. The Paczyński-Wiita potential (21) was first introduced in the paper by Paczyński & Wiita (1980). This is the most frequently cited paper by Bohdan on the subject of the black hole accretion. It ranks in the fourth place on the list of his most frequently cited papers. The figure and citation numbers were taken from the SAO/NASA ADS Astronomy Query service on June 6, 2008.

(i.e. Schwarzschild) black hole, the relativistic effective potential (16) takes the form (on the equatorial plane),

$$\mathcal{U}_{\text{Sch}} = -\frac{1}{2} \ln \left[\left(1 - \frac{r_G}{r} \right)^{-1} - \frac{\mathcal{L}^2}{r^2} \right], \quad (18)$$

and demanding that its first derivative is zero leads to the expression for the Keplerian angular momentum,

$$\mathcal{L}_K^2 = \frac{GM r^3}{(r - r_G)^2}. \quad (19)$$

Bohdan noticed that the same expression for the Keplerian angular momentum one gets for the effective potential given by the formula (on the equatorial plane),

$$\mathcal{U}_{PW} = -\frac{GM}{r - r_G} + \frac{\mathcal{L}^2}{2r^2}. \quad (20)$$

The second term on the right hand side, $\mathcal{L}^2/2r^2$, is the standard Newtonian centrifugal part of the effective potential. The first term should be therefore identified with a gravitational potential,

$$\Phi_{PW} = -\frac{GM}{r - r_G}, \quad (21)$$

which is indeed the celebrated “Paczynski-Wiita” or “pseudo-Newtonian” potential, first introduced by Bohdan in his paper with Paul Wiita (Paczyński & Wiita 1980).

3. The Doughnut

Several interesting phenomena that occur in black hole accretion disks have characteristic timescales t_* much shorter than the time $t_{\mathcal{L}}$ needed to redistribute the angular momentum, or the time $t_{\mathcal{S}}$ needed to redistribute the entropy

$$t_* \ll t_0 = \text{Min}(t_{\mathcal{L}}, t_{\mathcal{S}}) \quad (22)$$

During the time t_* , distributions of angular momentum and entropy,

$$\mathcal{L} = \mathcal{L}(r, \theta), \quad \mathcal{S} = \mathcal{S}(r, \theta) \quad (23)$$

do not change. The functions (23) cannot be unambiguously calculated from first principles, as they depend on unknown initial conditions, and on unknown details of dissipative processes such as e.g. turbulence, convection, or radiative transfer. Therefore, when they *are* calculated, for example with the help of lengthy and difficult numerical simulations, results *are arbitrary*, at least to some degree.

$$\left(\begin{array}{c} \text{step 1} \\ \text{arbitrary} \\ \text{assumptions} \end{array} \right) \rightarrow \left(\begin{array}{c} \text{step 2} \\ \text{difficult} \\ \text{calculations} \end{array} \right) \rightarrow \left(\begin{array}{c} \text{step 3} \\ \mathcal{L} = \mathcal{L}(r, \theta) \\ \mathcal{S} = \mathcal{S}(r, \theta) \end{array} \right) \quad (24)$$

Paczynski argued that there is no obvious reason to believe that it would be easier to guess what needs to be assumed in step 1 than to assume (guess) the result in the step 3. In the late 1970s and early 1980s he and his collaborators explored accretion disk models in which distributions of angular momentum and entropy (23) were assumed ad hoc.

For a perfect-fluid matter, $T^i_k = (p + \epsilon)u^i u_k - p\delta^i_k$, with p and ϵ being the pressure and the total energy density. Equations of mass conservation and energy-momentum conservation take the form,

$$\nabla_i(u^i \rho) = 0, \quad \nabla_i T^i_k = 0, \quad (25)$$

where ρ is the rest-mass density. From these equations one deduces that two Bernoulli-type quantities are constant along the stream-lines of the perfect fluid matter moving in a stationary and axially symmetric spacetime (1)-(2).

$$\mathcal{B}^* = \left(\frac{p + \epsilon}{\rho} \right) u_t, \quad \mathcal{L}^* = - \left(\frac{p + \epsilon}{\rho} \right) u_\phi \quad (26)$$

Thus, the purely kinematic quantity, defined previously as the specific angular momentum for particles,

$$\mathcal{L} = \frac{\mathcal{L}^*}{\mathcal{B}^*} = - \frac{u_\phi}{u_t}, \quad (27)$$

is also constant along fluid's stream-lines. If the fluid moves along circular stream-lines (12), the equation of motion $\nabla_i T^i_k = 0$ yields (c.f. equation (16)),

$$\frac{\nabla_i p}{p + \epsilon} = - \frac{1}{2} \frac{\nabla_i g^{tt} - 2\mathcal{L} \nabla_i g^{t\phi} + \mathcal{L}^2 \nabla_i g^{\phi\phi}}{g^{tt} - 2\mathcal{L} g^{t\phi} + \mathcal{L}^2 g^{\phi\phi}} = \left(\frac{\partial \mathcal{U}_{\text{Kerr}}}{\partial x^i} \right)_{\mathcal{L}}, \quad (28)$$

which may be transformed into,

$$\frac{\nabla_i p}{p + \epsilon} = \nabla_i \mathcal{U} + \frac{\Omega \nabla_i \mathcal{L}}{1 - \mathcal{L} \Omega}. \quad (29)$$

Here $\Omega = u^\phi/u^t$ is the angular velocity, related to the angular momentum \mathcal{L} by the following formulae, which are very useful in practical calculations.

$$\mathcal{L} = -\frac{\Omega g_{\phi\phi} + g_{t\phi}}{\Omega g_{t\phi} + g_{tt}}, \quad \Omega = -\frac{\mathcal{L} g_{tt} + g_{t\phi}}{\mathcal{L} g_{t\phi} + g_{\phi\phi}} \quad (30)$$

3.1. The von Zeipel fluid tori

Suppose that $p = p(\epsilon)$, as it would be for isentropic, polytropic or barytropic fluid. In this case, the left hand side of equation (29) is a perfect gradient, and so must be the right hand side, and this is possible when $\mathcal{L} = \mathcal{L}(\Omega)$. Similarly, if $\mathcal{L} = \mathcal{L}(\Omega)$, then the right hand side is a gradient, and so must be the left hand side. This statement is known as the von Zeipel condition,

$$[p = p(\epsilon)] \Leftrightarrow [\mathcal{L} = \mathcal{L}(\Omega)], \quad (31)$$

or, the $p(r, \theta) = \text{const}$ surfaces coincide with those of $\epsilon(r, \theta) = \text{const}$, *if and only if* the surfaces $\mathcal{L}(r, \theta) = \text{const}$ coincide with those $\Omega(r, \theta) = \text{const}$ ³.

The simplest example of a fluid fulfilling the von Zeipel condition (31) is

$$\mathcal{L}(r, \theta) = \mathcal{L}_0 = \text{const}, \quad \mathcal{S}(r, \theta) = \mathcal{S}_0 = \text{const}. \quad (32)$$

In this case, equation (29) has a trivial first integral

$$W(p) = \mathcal{U}_{\text{Kerr}}(r, \theta), \quad (33)$$

where $W(p)$ is the enthalpy, defined for isentropic fluids (32) by

$$W = W(p) = \int \frac{dp}{p + \epsilon}. \quad (34)$$

Note that (33) gives the location of the isobaric surfaces in terms of an *explicit* analytic function of coordinates r, θ . From (28) it follows that the pressure maximum is located at the circle $r = r_0, \theta = \theta_0 = \pi/2$, given by the condition,

$$\left(\frac{\partial \mathcal{U}_{\text{Kerr}}}{\partial r} \right)_{\mathcal{L}} = 0 = \left(\frac{\partial \mathcal{U}_{\text{Kerr}}}{\partial \theta} \right)_{\mathcal{L}}. \quad (35)$$

Let us express the effective potential near the pressure maximum circle r_0, θ_0 by

$$\Delta \mathcal{U} = \mathcal{U}_{\text{Kerr}}(r, \theta) - \mathcal{U}_{\text{Kerr}}(r_0, \theta_0). \quad (36)$$

Because the first derivative of the effective potential vanishes at the maximum pressure circle, and the second derivatives equal to the epicyclic frequencies (c.f.

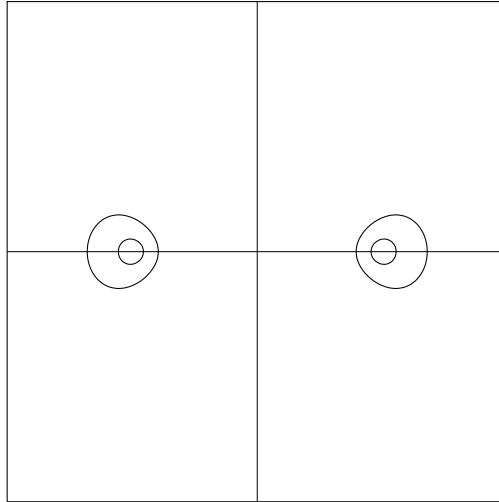


Figure 3. Contours of equipotential surfaces on the meridional cross section of a torus with constant angular momentum, exactly calculated from (33), according to Newton’s theory with the $-GM/r$ gravitational potential. The contours approach circles around the locus of the maximum pressure, at the $r = r_0$, $\theta = \theta_0 = \pi/2$ circle, which agrees with the approximate “slender torus” solution given by equation (37).

equation (11)), one concludes that the shape of a “slender” torus, i.e. with $\Delta r \equiv r - r_0 \ll r_0$, $\Delta\theta \equiv \theta - \theta_0 \ll \theta_0$, is given by $\Delta\mathcal{U} = \text{const}$, with

$$\Delta\mathcal{U}(r, \theta) = \frac{1}{2} \left[\omega_r^2 (\Delta r)^2 + \omega_\theta^2 (\Delta\theta)^2 \right] + \mathcal{O}^3(\varepsilon), \quad \varepsilon = \frac{\Delta r}{r_0} \ll 1. \quad (37)$$

Equation (37) is valid both in Newton’s and Einstein’s theory. In Newton’s theory with $-GM/r$ gravitational potential, one has $\omega_r = \omega_\theta$. Thus, in this case, one concludes from equation (37) that slender constant-angular-momentum fluid tori have *circular* cross-sections. This additional symmetry was first noticed by Bohdan in his paper with Jurek Madej (Madej & Paczyński 1977), and later used by Blaes (1985) to calculate normal modes of oscillations of slender tori. Blaes demonstrated that there exists a set of non-axisymmetric (i.e. with $m \neq 0$) global modes $\delta\Psi_{mn} \sim \exp(-i\sigma_{mn}t + m\phi)$ with the eigenfrequencies,

$$\sigma_{mn} = -m\Omega_K \left[1 + i\epsilon \left(\frac{3}{2n+2} \right)^{\frac{1}{2}} \right] + \mathcal{O}^2(\epsilon), \quad n = 1, 2, 3, \dots \quad (38)$$

Because $\Im(\sigma_{mn}) < 0$ these oscillations are unstable. The growth rate of the instability is $\sim m\Omega_K$, and thus the instability is a *dynamical* one. Indeed, this

³The best known Newtonian version of the von Zeipel condition states that for a barytropic fluid $p = p(\epsilon)$, both angular velocity and angular momentum are constant on cylinders, $\Omega = \Omega(R)$, $\mathcal{L} = \mathcal{L}(R)$, with $R = r \sin \theta$ being the distance from the rotation axis.

is the famous Papaloizou-Pringle instability, discovered in the seminal paper by John Papaloizou and James Pringle (Papaloizou & Pringle 1984).

In the last twenty years, studies of slender tori oscillations have brought a lot of important results. Today, these results are concentrated in non-linear excitation, damping, and resonances of global epicyclic modes that are thought to be relevant to the 3:2 twin peak QPOs. The velocity pattern for the vertical epicyclic mode of a slender torus in the Kerr geometry is shown in Figure 4, taken from Straub & Šramková (2008).

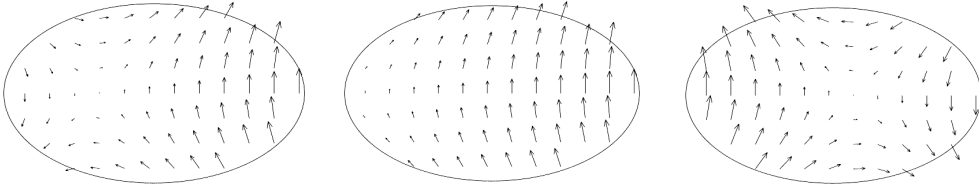


Figure 4. Velocity pattern for the vertical epicyclic mode of oscillation of a slender torus around a Kerr black hole as calculated from an analytic model by Straub & Šramková (2008).

3.2. General case

Jaroszyński & al (1980) discuss a general, non-barytropic case of angular momentum and entropy distributions (23). They start by noting that if $\theta = \theta(r)$ is the equation for the isobaric surface $p(r, \theta) = \text{const}$, then obviously

$$\frac{d\theta}{dr} = -\frac{\partial_r p}{\partial_\theta p}. \quad (39)$$

They further note that the right hand side of the above equation may be calculated from (28), if one writes it twice for $i = r$ and $i = \theta$, divides the two equations, and changes the sign,

$$-\frac{\partial_r p}{\partial_\theta p} = -\frac{\partial_r g^{tt} - 2\mathcal{L} \partial_r g^{t\phi} + \mathcal{L}^2 \partial_r g^{\phi\phi}}{\partial_\theta g^{tt} - 2\mathcal{L} \partial_\theta g^{t\phi} + \mathcal{L}^2 \partial_\theta g^{\phi\phi}}. \quad (40)$$

The point here is that because the Kerr metric g^{ik} is known explicitly in terms of r and θ , and because the distribution of the angular momentum is given by the assumption (23), the right hand side of (40) is an explicitly known function of r and θ . One may denote this function by $F(r, \theta)$, and combine equations (39) and (40) into the standard form of an ordinary differential equation,

$$\frac{d\theta}{dr} = F(r, \theta), \quad (41)$$

with the explicitly known right hand side. It may be directly integrated to get all possible locations of the isobaric surfaces.

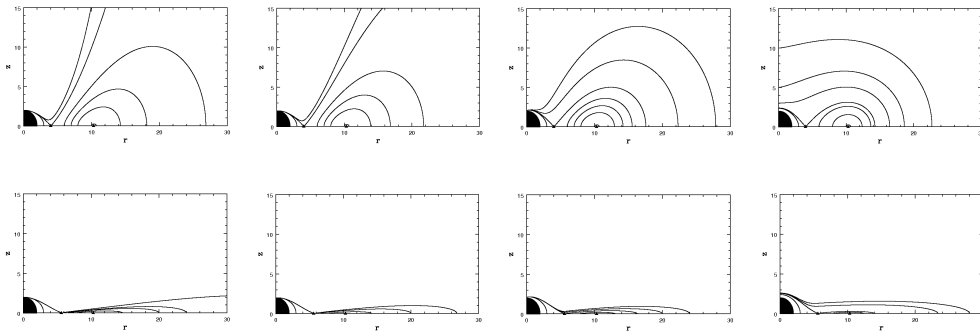


Figure 5. Shapes of Polish doughnuts. Upper row: for almost constant angular momentum, $\beta \approx 0$. Lower row: for almost Keplerian angular momentum, $\beta \approx 1$. The parameter γ increases in equal steps from left, $\gamma = 0$, to right, $\gamma = 1$.

Qian & al (2008) have recently argued that a physically flexible and realistic angular momentum distribution may be assumed of the form,

$$\mathcal{L}(r, \theta) = \left\{ \begin{array}{l} \mathcal{L}_0 \left(\frac{\mathcal{L}_K(r)}{\mathcal{L}_0} \right)^\beta (\sin \theta)^{2\gamma} \quad \text{for } r > r_{ms} \\ \mathcal{L}_{ms} (\sin \theta)^{2\gamma} \quad \text{for } r < r_{ms} \end{array} \right\}, \quad (42)$$

where $\mathcal{L}_{ms} \equiv \mathcal{L}_0 [\mathcal{L}_K(r_{ms})/\mathcal{L}_0]^\beta$, and \mathcal{L}_0 , β , and γ are the three free constant parameters of the distribution. Figure 5 shows several models calculated for different choices of $\mathcal{L}_0, \beta, \gamma$.

Recently Komissarov (2006) constructed models of magnetized Polish doughnuts.

4. The Funnel

Long, narrow funnels along the axis are a genuine feature of Polish doughnuts. Bohdan realized that they may be relevant for beaming radiation to highly super-Eddington fluxes and collimating relativistic jets.

4.1. Super-Eddington luminosities in funnels

In this section, I will use Newton's theory and cylindrical coordinates r, z, ϕ . In Newton's theory, the first integral (33) that describes equilibrium of the constant angular momentum, constant entropy fluid takes the form,

$$-\frac{GM}{(r^2 + z^2)^{\frac{1}{2}}} + \frac{1}{2} \frac{\mathcal{L}^2}{r^2} + W(p) = \text{const.} \quad (43)$$

This equation cannot be obeyed at the rotation axis (where $z \neq 0, r = 0$), which has an obvious, but important, consequence: no isobaric surface may cross the axis. For a constant angular momentum fluid, isobaric surfaces must be toroidal,

or open. The marginally open surface has just one point ($r = \infty, z = 0$) at infinity. This particular surface encloses the *largest possible* torus. From (43) it is obvious that in this case $W(p) = W(0) = 0$. The maximal pressure is located at a circle $z = 0, r = r_0 = GM/\mathcal{L}_0^2$. Using the radius r_0 as a scale, $\xi = r/r_0$, $\eta = z/r_0$, $w = W/(GM/r_0)$, one may write equation (43) in the dimensionless form, and solve for $\eta = \eta(\xi, w)$ to obtain,

$$\eta^2 = Q^2(\xi) \equiv 4\xi^4 (1 - 2\xi^2 w)^{-2} - \xi^2, \quad -1/2 \leq w \leq w_S. \quad (44)$$

The value $w = -1/2$ gives the location of the center, and $w = w_S \leq 0$ the location of the surface. For the *slender torus* $w_S \approx -1/2$, and the *fat torus* $w_S \approx 0$. Very far from the axis of rotation one has $|2w\xi| \gg 1$. Inserting this

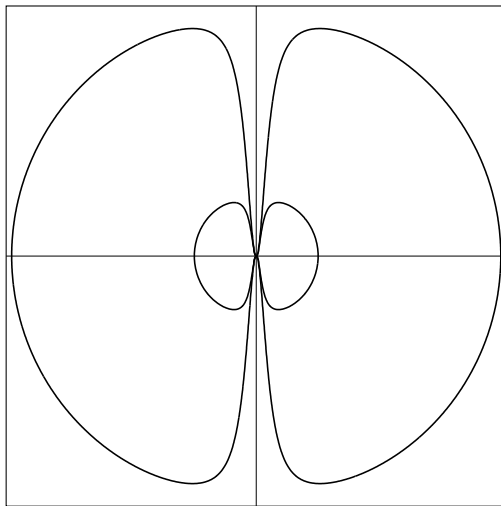


Figure 6. Contours of equipotential surfaces on the meridional cross section of a fat torus with constant angular momentum, i.e. with $w_s \approx 0$. Close to axis the isobaric surfaces form a pair of conical funnels.

into (44) one gets $\eta^2 + \xi^2 = 1/w^2$ which means that far from the rotation axis the equipotential surfaces are spheres with radius $1/|w|$, and that the outer radius of the torus is at $r_{\text{out}} = r_0/|w_S|$. Spherical equipotentials are in accord with the fact that very far from the axis, $\xi \gg 1$, the centrifugal force $\sim \mathcal{L}_0^2/\xi^3$ is negligible with respect to the gravitational force $\sim GM/\xi^2$. Therefore, the effective gravity is determined by Newton's attraction alone, as for spherical stars. For the same reason, the radiation power from this part of the surface of a fat, radiation-pressure-supported torus (i.e. Polish doughnut) is *one Eddington luminosity*, the same as from a spherical non-rotating, radiation-pressure-supported star⁴.

⁴Martin Rees told me as early as 1980 that to him this implied that Polish doughnuts, with at least one Eddington luminosity from whatever direction, were obviously too luminous to describe very "dim" active galactic nuclei, such as radio galaxies: "while apparently supplying tremendous power to their extended radio-emitting regions, the nuclei of most radio galaxies

Note, however, that the asymptotically spherical shape of a fat torus is a direct consequence of the assumption $\mathcal{L}(r, z) = \text{const}$, which was made ad hoc. If one adopts a more physically realistic assumption that asymptotically $\mathcal{L}(r, z) = \mathcal{L}_K$, as in our model (42), one may use the standard Shakura-Sunyaev model in its radiation pressure version to get the asymptotic shape of the fat torus,

$$z_\infty = \frac{3\sigma_T}{8\pi c m_p} \dot{M}. \quad (45)$$

Closer to the axis, $|2w\xi| \sim 1$, which means that $\xi^2 \sim -1/2w$, and this together with (44) gives $\eta^2/\xi^2 = (1/|w|) - 1 = (1/\sin^2\theta) - 1$, i.e. that closer to the axis, equipotential surfaces corresponding to $w \sim w_S \sim 0$ have conical shapes with the half opening angle $\theta \sim \sqrt{|w|}$. The surfaces are highly non-spherical because centrifugal force dominates. Integrating effective gravity along the conical funnel is elementary, and one gets (Jaroszyński & al 1980) that $L_{\text{Edd}}^{\text{rot}}/L_{\text{Edd}} = (1/2) \ln(1/|w_S|)$. This estimate may be used to find the total luminosity for the radiation-pressure-supported fat torus. i.e. a Polish doughnut,

$$\frac{L_{\text{total}}}{L_{\text{Edd}}} \approx \frac{L_{\text{Edd}}^{\text{rot}}}{L_{\text{Edd}}} \approx \frac{1}{2} \ln\left(\frac{r_{\text{out}}}{r_0}\right) = 1.15 \log\left(\frac{r_{\text{out}}}{r_0}\right). \quad (46)$$

It should be clear from our derivation that the logarithmic scaling of the luminosity with the torus size is a genuine property of Polish doughnuts, including those that have an angular momentum distribution that is not constant. The logarithm in (46) is of crucial importance, as it prevents astrophysically realistic doughnuts (i.e. with $r_{\text{out}}/r_0 < 10^6$, say) from having highly super-Eddington luminosities. Thus, the theory predicts that for such “realistic” fat tori, only slightly super-Eddington total (isotropic) luminosities, $L_{\text{total}} \geq 7 L_{\text{Edd}}$, may be expected.

However, because the funnels have solid angles $\theta^2 \sim r_0/r_{\text{out}}$, radiation in the funnels may be, in principle, collimated to highly super-Eddington values $L_{\text{coll}}/L_{\text{Edd}} = \Theta \sim r_{\text{out}}/r_0 \gg 1$. This simple estimate agrees with a more detailed modelling of the radiation field of the Polish doughnuts by Sikora (1981) and Madau (1988) who obtained $\Theta \leq 10^2$ for disks with $r_{\text{out}}/r_0 \sim 10^2$. A typical value that follows from observational estimates for non-blazar active galactic nuclei (e.g. Malkan 1989; Czerny & Elis 1987) is $\Theta \sim 10$, but of course for blazars and other similar sources, e.g. for ULXs, if they are powered by stellar mass black holes, as argued by King (2002), it must be $\Theta \gg 10$.

Such high values of Θ are also consistent with the idea, suggested by Paczyński (1980) and independently by Lynden-Bell (1982), that relativistic electron-positron e^-e^+ jets may be very effectively accelerated by the radiation pressure in the fat tori funnels⁵. Note that if the flux in the funnel is Θ times

emit little detectable radiation.” He and his collaborators at Cambridge later found a possible solution to this puzzle in terms of the *ion-pressure-supported tori* Rees & al (1982). The ion tori have the same shapes as Polish doughnuts (in particular funnels) but have much lower, indeed very sub-Eddington, luminosities. The power in jets comes from tapping the rotational energy of the central black hole by the Blandford-Znajek mechanism Blandford & Znajek (1977).

⁵Lynden-Bell called this an “entropy fountain”.

the Eddington flux, the e^-e^+ plasma feels the “effective” radiative force corresponding to the Eddington ratio $m_p/m_e \approx 10^3$ times greater. Detailed calculations (e.g. Abramowicz & Piran 1980; Sikora & Wilson 1981; Abramowicz & al 1990) demonstrate that indeed the e^-e^+ jets may be accelerated in funnels up to the Lorentz factor $\gamma \leq 5$. However, if jets are initially pre-accelerated by some black-hole electro-dynamical processes (such as the Blandford-Znajek mechanism, Blandford & Znajek 1977) to highly relativistic velocities $\gamma > 10^6$, they will be decelerated in the funnels by Compton drag, reaching the asymptotic Lorentz factor (Abramowicz & al 1990),

$$\gamma_\infty = \left(\Theta \frac{m_p}{m_e} \right)^{\frac{1}{3}} = 10 \times \Theta^{\frac{1}{3}}. \quad (47)$$

Observations show that $\gamma_\infty < 10^2$, and thus equation (47) suggests that $\Theta < 10^3$.

4.2. The physical reason for super-Eddington luminosities

I will now review a very general argument, first presented by Abramowicz, Calvani & Nobili (1980), which shows that the upper limit for the luminosity of rotating bodies in equilibrium must differ from the Eddington limit. I will consider two “astrophysical” cases:

Rotating stars. The surface of the star has the topology of a sphere. The whole mass M is included in the sphere.

Accretion disks. The surface of the disk has the topology of a torus. The mass of the disk M_{disk} is contained in the torus, but the mass M_{centr} of the central black hole is outside. The total mass $M = M_{\text{centr}} + M_{\text{disk}} \approx M_{\text{centr}}$, because $M_{\text{centr}} \gg M_{\text{disk}}$. In accretion disk theory it is customary to neglect the mass of the disk, so formally $M = M_{\text{centr}}$, and $M_{\text{disk}} = 0$. The Eddington limit always refers to the total mass M .

Let \mathbf{f}_{rad} be the local flux of radiation somewhere at the surface of the body, S . The corresponding radiative force is $\mathbf{F}_{\text{rad}} = (\sigma_{\text{rad}}/c)\mathbf{f}_{\text{rad}}$. Let $\mathbf{F}_{\text{eff}} = \mathbf{F}_{\text{grav}} + \mathbf{F}_{\text{rot}}$, be the effective gravitational force, with $\mathbf{F}_{\text{grav}} = m\nabla\Phi$ being the gravitational force (Φ is the gravitational potential), and with $\mathbf{F}_{\text{rot}} = m(\Omega^2 r)\mathbf{e}_r$ being the centrifugal force (Ω is the angular velocity, r is the distance from the axis of rotation, and $\mathbf{e}_r = \nabla r$ a unit vector in the off-axis direction).

The necessary condition for equilibrium is $\mathbf{F}_{\text{rad}} < \mathbf{F}_{\text{eff}}$. From this one deduces the Eddington limit for rotating perfect-fluid bodies,

$$L = \int_S \mathbf{f}_{\text{rad}} \cdot d\mathbf{S} = \frac{c}{\sigma_{\text{rad}}} \int_S \mathbf{F}_{\text{rad}} \cdot d\mathbf{S} < \frac{c}{\sigma_{\text{rad}}} \int_S \mathbf{F}_{\text{eff}} \cdot d\mathbf{S} \equiv L_{\text{Edd}}^{\text{rot}} \quad (48)$$

Using Gauss’s theorem to transform the surface integral of \mathbf{F}_{eff} into a volume integral of $\nabla \cdot \mathbf{F}_{\text{eff}}$, Poisson’s equation $\nabla^2\Phi = 4\pi G\rho$, and introducing the specific angular momentum $\ell = \Omega r^2$, one gets after twenty or so lines of simple algebra,

$$L_{\text{Edd}}^{\text{rot}} = L_{\text{Edd}} \left[X_{\text{mass}}^2 + X_{\text{shear}}^2 - X_{\text{vorticity}}^2 \right], \quad (49)$$

where L_{Edd} is the standard Eddington limit for a non-rotating star,

$$L_{\text{Edd}} = 1.4 \times 10^{38} \left(\frac{M}{M_\odot} \right) [\text{erg sec}^{-1}]. \quad (50)$$

and where the dimensionless number X_{mass}^2 depends on whether the body is a star, or an accretion disk,

$$X_{\text{mass}}^2 = \frac{1}{M} \int_V \rho dV = \left\{ \begin{array}{l} 1 \text{ for stars,} \\ 0 \text{ for accretion disks,} \end{array} \right\}. \quad (51)$$

Here X_{shear}^2 and $X_{\text{vorticity}}^2$ are dimensionless, necessarily positive quantities, equal to shear and vorticity integrated over the whole volume of the body,

$$X_{\text{shear}}^2 = \frac{1}{16\pi GM} \int_V r^2 (\nabla\Omega \cdot \nabla\Omega) dV, \quad (52)$$

$$X_{\text{vorticity}}^2 = \frac{1}{16\pi GM} \int_V r^{-2} (\nabla\mathcal{L} \cdot \nabla\mathcal{L}) dV. \quad (53)$$

Shear increases the Eddington limit, and vorticity decreases it.

The rotation of astrophysical objects is far from simple, but insight can be gained by considering a simple power law for the angular momentum distribution, $\mathcal{L}(r, z) = \mathcal{L}_0 r^a$, with \mathcal{L}_0 and a constant. Rigid rotation has $a = 2$, Keplerian rotation $a = 1/2$, and constant angular momentum rotation $a = 0$. X_{shear} and $X_{\text{vorticity}}$ are related to a by $X_{\text{shear}}^2/X_{\text{vorticity}}^2 = (a - 3)^2/a^2$. This means that $X_{\text{shear}}^2 > X_{\text{vorticity}}^2$ when $a < 3/2$.

Rotating stars have $X_{\text{shear}}^2 < X_{\text{vorticity}}^2$, because they rotate almost rigidly. Thus, for rotating, radiation pressure supported stars, $L \approx L_{\text{Edd}}^{\text{rot}} < L_{\text{Edd}}$ *always*. Contrary to this, tori with constant angular momentum are dominated by shear, $X_{\text{shear}}^2 \gg 1 \gg X_{\text{vorticity}}^2$ and consequently, when they are radiation pressure supported, $L \approx L_{\text{Edd}}^{\text{rot}} \gg L_{\text{Edd}}$.

4.3. Rise and Fall of the Polish Doughnuts

At the time of their *début*, Polish doughnuts could theoretically confirm the observed super-Eddington luminosities, highly collimated beams of radiation, and perhaps even the relativistic speeds of jets, fulfilling the principle attributed to Eddington: *one should never believe any experiment until it has been confirmed by theory*. These virtues initially attracted some interest in the astrophysical community, but the interest quickly drained with the discovery of the Papaloizou-Pringle instability. It was thought that Polish doughnuts must necessarily suffer from the instability and thus, in reality, they cannot exist. The important discovery by Blaes (1987) that the Roche lobe overflow stabilizes Polish doughnuts against the Papaloizou-Pringle instability came too late — in the advent of numerical simulations of black hole accretion flows. Too late, because numerical simulations rediscovered and absorbed many of the results of Polish doughnuts. Today, these results exist in the consciousness of many astrophysicists as a set of several numerically established, important but unrelated facts. They do not form a consistent scheme that the Polish doughnuts once offered: clear, simple, following directly from the black hole physics⁶.

⁶There are at least three brilliant and very pedagogical expositions of the Polish doughnuts scheme: two by Paczyński himself (Paczyński 1982, 1998) and one in the text book by Frank, King & Raine (2002).

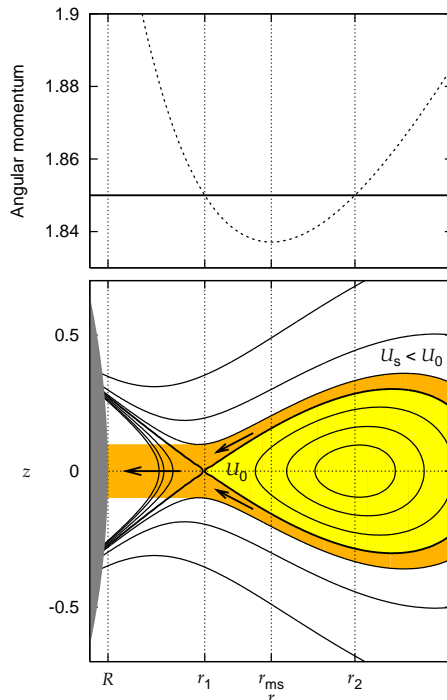


Figure 7. Upper figure shows the Keplerian angular momentum (the dotted line) and the angular momentum in the flow (the solid line). Lower figure shows the equipotential surfaces (solid lines) and distribution of fluid (shade).

5. The Roche Lobe

A powerful analytic model for accretion flows near the ISCO was worked out in terms of the flow equipotential structure by Paczyński and collaborators thirty years ago in Warsaw (see e.g. Abramowicz & al 1978; Kozłowski & al 1978; Jaroszyński & al 1980; Abramowicz 1981). The Warsaw model accurately describes the flow hydrodynamics for the standard Shakura-Sunyaev thin disks, slim disks, adafs, ion tori, and thick Polish doughnuts. It impressively agrees with more recent numerical simulations of accretion flows, as directly checked e.g. by Igumenshchev & Abramowicz (2000).

In an equilibrium described by the Bernoulli equation (43), surfaces of constant enthalpy, pressure and density coincide with surfaces of constant effective potential, $\mathcal{U}(r, z) = \text{const}$. The surface of the disk is given by $P = \text{const} = 0$. Thus, equilibria may only exist if the disk surface corresponds to one of the equipotentials inside the Roche lobe, i.e. in the region indicated by yellow in Figure 7. If the fluid distribution overflows the Roche lobe, i.e. the surface of the disk for $r \gg r_1$ coincides with $\mathcal{U}(r, z) = \mathcal{U}_s < \mathcal{U}_0$, the equilibrium in the region $r \leq r_1$ is not possible, and the disk will suffer a dynamical mass loss, with accretion rate \dot{M}_{in} .

5.1. The stationary Roche lobe overflow

An analytic formula for \dot{M} for stationary flows was first calculated by Kozłowski & al (1978), who used Einstein's theory. Here we review another derivation, done by Abramowicz (1985), as we later use the same assumptions and notation to calculate \dot{M} for a non-stationary (oscillating) disk. In particular, we assume that the Roche lobe overflow is small (quadratic in disk thickness H),

$$h(r_1, z) = h^* - \frac{1}{2}\kappa^2 z^2, \quad \kappa^2 \equiv - \left(\frac{\partial^2 h}{\partial z^2} \right)_L, \quad H = \frac{\sqrt{2h^*}}{\kappa}, \quad (54)$$

that the equation of state is polytropic, and that the radial velocity v^r connected to the mass loss through the cusp equals the sound speed c_s ,

$$P = K\rho^{1+1/n}, \quad v^z \ll v^r = c_s = \sqrt{\frac{h}{n}}. \quad (55)$$

In the equations above $h^* = h(r_1, 0)$ denotes a maximal value of the enthalpy on the cylinder $r = r_1$ and the subscript L stands for the evaluation of the derivative at the point $[r_1, 0]$. The local mass flux $\dot{m} = \rho v^r = h^{n+1/2}/K^n(1+n)^n n^{1/2}$, vertically integrated through the cusp thickness and azimuthally around, gives the desired total mass flux in terms of the enthalpy,

$$\begin{aligned} \dot{M} &= \int_0^{2\pi} r_1 d\varphi \int_{-H}^{+H} \dot{m} dz = \\ &= (2\pi)^{3/2} \frac{r_1}{\kappa n^{1/2}} \left[\frac{1}{K(n+1)} \right]^n \frac{\Gamma(n+3/2)}{\Gamma(n+2)} h_0^{n+1}. \end{aligned} \quad (56)$$

Here $\Gamma(x)$ is the Euler gamma function. From $v^2/2 + h + \mathcal{U} = \mathcal{U}_S$ one gets $\Delta\mathcal{U} = \mathcal{U}_S - \mathcal{U} = (1 + 1/2n)h$ and from

$$\kappa^2 \equiv - \left(\frac{\partial^2 h}{\partial z^2} \right)_L \left(\frac{n}{n+1/2} \right) \omega_z^2, \quad \omega_z^2 \equiv \left(\frac{\partial^2 \mathcal{U}}{\partial z^2} \right)_L, \quad (57)$$

we recover the result obtained by Abramowicz (1985),

$$\dot{M} = A(n) \frac{r_1}{\omega_z} \Delta\mathcal{U}^{n+1}, \quad (58)$$

$$A(n) \equiv (2\pi)^{3/2} \left[\frac{1}{K(n+1)} \right]^n \left[\frac{1}{n+1/2} \right]^{n+1/2} \frac{\Gamma(n+3/2)}{\Gamma(n+2)}. \quad (59)$$

Figure 5.1. shows an excellent agreement between the analytic formula (58) and results of large-scale, 3D, non-stationary numerical simulations.

5.2. Non-stationary Roche lobe overflow

We will calculate \dot{M} for non-stationary oscillating flows in a special but important case, assuming that the poloidal part of velocity $\vec{v} = (v^r, v^z)$ may be

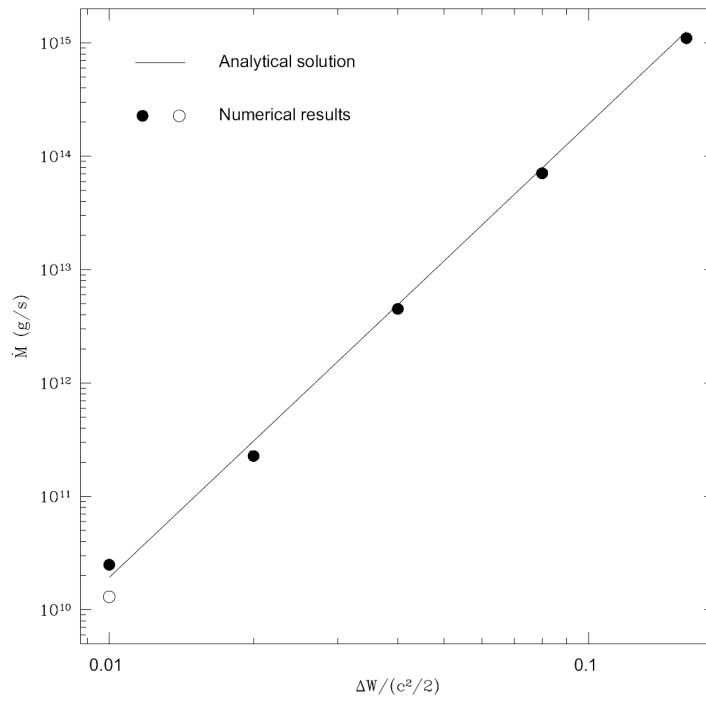


Figure 8. The line is according to the analytic formula (58) and the points are from non-stationary, 3D numerical simulations by Igumenshchev & Abramowicz (2000).

derived from a potential. In this case, the non-stationary version of the Bernoulli equation has the form,

$$\frac{\partial \chi}{\partial t} + \frac{v^2}{2} + h + \mathcal{U}\mathcal{U}_S, \quad \text{with} \quad \vec{v} = \nabla \chi. \quad (60)$$

We assume that the oscillation is a small, non-stationary perturbation to the stationary flow considered in the previous section,

$$\chi(\vec{r}, t) = \chi_{(0)}(\vec{r}) + \epsilon \chi_{(1)}(\vec{r}, t), \quad (61)$$

where the subscript (0) refers to the stationary flow and the dimensionless parameter $\epsilon \ll 1$ characterizes the strength of the perturbation. From the definition $\vec{v} = \nabla \chi$ one derives,

$$\begin{aligned} v^2 &= v_{(0)}^2 + 2\epsilon \vec{v}_{(0)} \cdot \vec{v}_{(1)} + \epsilon^2 v_{(1)}^2 \\ &= c_s^2 + 2\epsilon c_s \frac{\partial \chi_{(1)}}{\partial r} + \epsilon^2 \left[\left(\frac{\partial \chi_{(1)}}{\partial r} \right)^2 + \left(\frac{\partial \chi_{(1)}}{\partial z} \right)^2 \right]. \end{aligned} \quad (62)$$

The perturbed enthalpy profile can be approximated by an expansion

$$h = h_{(0)} + \epsilon h_{(1)} + \epsilon^2 h_{(2)} + \mathcal{O}(\epsilon^3). \quad (63)$$

By substituting equations (62) and (63) into the Bernoulli equation (60) and equating coefficients of the same powers of ϵ , we get

$$h_{(1)} = -\frac{\partial \chi_{(1)}}{\partial t} - \left(\frac{\bar{h}}{n} \right)^{1/2} \frac{\partial \chi_{(1)}}{\partial r}, \quad (64)$$

$$h_{(2)} = -\frac{1}{2} \left[\left(\frac{\partial \chi_{(1)}}{\partial r} \right)^2 + \left(\frac{\partial \chi_{(1)}}{\partial z} \right)^2 \right]. \quad (65)$$

This way, we express perturbations of fluid quantities in terms of a perturbation $\chi_{(1)}$. To progress further, one must know the function $\chi_{(1)} = \chi_{(1)}(t, r, z)$ that describes oscillations. Finding it in general is a difficult global problem. We do not attempt to solve it here. Instead, we describe oscillations by an ansatz,

$$\chi_{(1)} = z v_z \cos \omega t, \quad v_z = \text{const}. \quad (66)$$

which models a vertical ‘‘epicyclic’’ oscillation with frequency ω that rigidly moves the fluid up and down across the equatorial symmetry plane. Such a rigid mode, with the eigenfrequency equal to the epicyclic vertical frequency, $\omega = \omega_z$, has been recently identified by Abramowicz & al (2006) as a combination of eigenmodes of slender torus oscillations found previously by Blaes (1985). This classic paper gives *all* possible modes, i.e. their eigenfrequencies and eigenfunctions, in terms of exact, simple, and explicit analytic formulae.

The quantity $\epsilon v_z = \text{const}$ can be interpreted as the amplitude of the vertical velocity. Equations (64) and (65) give

$$h_{(1)} = z v_z \omega \sin \omega t, \quad h_{(2)} = -\frac{1}{2} v_z^2 \cos^2 \omega t. \quad (67)$$

The vertical profile of the enthalpy at $r = r_1$ is

$$\begin{aligned} h(r_1, z, t) &= h^* - \kappa^2 z^2 + \epsilon z v_z \omega \sin \omega t - \\ &\quad - \frac{1}{2} \epsilon^2 v_z^2 \cos^2 \omega t + \mathcal{O}(\epsilon^3), \end{aligned} \quad (68)$$

which is quadratic in the variable z (see the left panel of Fig. 9). The position of the enthalpy maximum on the cylinder $r = r_1$ is shifted from $z = 0$ to height $\delta z(t)$, given as

$$\delta z(t) = \delta Z \sin \omega t, \quad \delta Z = \epsilon \frac{\omega v_z}{\kappa^2}. \quad (69)$$

We can interpret δZ as the amplitude of the oscillations. Also the value of enthalpy in the maximum differs from the stationary case by

$$\begin{aligned} \delta h^* &\equiv h(r_1, \delta z) - h^* \\ &= \frac{1}{2} \kappa^2 \left[\delta z^2 - \frac{\kappa^2}{\omega^2} (\delta Z^2 - \delta z^2) \right] + \mathcal{O}(\epsilon^3). \end{aligned} \quad (70)$$

According to equation (56) the instantaneous accretion rate depends on the maximal enthalpy as $\dot{M} \propto (h^*)^{n+1}$. This relation can also be applied in the case of vertical oscillations because the z -dependence of enthalpy on the cylinder $r = r_1$ remains quadratic and the oscillations do not contribute to the radial velocity of accreted matter. Hence, using equations (54), (57) and (70) and assuming that the frequency of oscillations equals the local vertical epicyclic frequency, $\omega = \omega_z$, we arrive at our final result

$$\begin{aligned} \frac{\delta \dot{M}}{\dot{M}_{(0)}} &= (n+1) \frac{\delta h^*}{h^*} \\ &= \frac{2-p}{2-2p} \left[(1+p) \frac{\delta z^2}{H^2} - p \frac{\delta Z^2}{H^2} \right], \end{aligned} \quad (71)$$

where $\delta \dot{M} \equiv \dot{M} - \dot{M}_{(0)}$ and $p \equiv n/(n+1/2)$. The quadratic dependence of $\delta \dot{M}$ on perturbation implies that the frequency of modulation of \dot{M} is twice the frequency of the disk oscillation (see the right panel of Fig. 9).

6. The Inner Edge

This is a very controversial point of a *fundamental* importance. In Bohdan's own words (Afshordi & Paczyński 2003), "Theory of accretion disks is several decades old. With time ever more sophisticated and more diverse models of accretion onto black holes have been introduced. *However, when it comes to modeling disk spectra, conventional steady state, geometrically thin-disk models are still used, adopting the classical "no torque" inner boundary condition at the marginally stable orbit at the ISCO.* (e.g. Blaes & al 2001). Recently, the no torque condition for geometrically thin disks has been challenged by several authors (Krolik 1999; Gammie 1999; Agol & Krolik 2000). I did not agree with

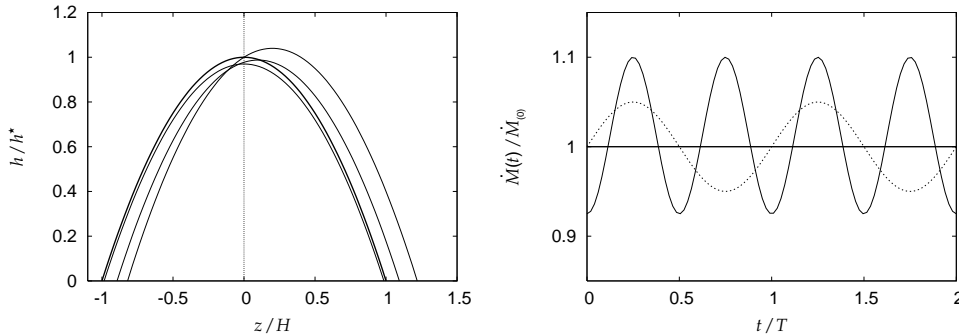


Figure 9. Left: The vertical profiles of the enthalpy $h(r_1, z)$ on the cylinder $r = r_1$ during vertical disk oscillations (thin lines). The amplitude of oscillations is $\delta Z = 0.2H$ and we chose the polytropic index of the fluid $n = 1.5$. The figure captures profiles with enthalpy maxima at $\delta z = 0, 0.1H$ and $0.2H$. The enthalpy profile for the unperturbed stationary disk is also shown (thick line). Right: The modulated accretion rate from the oscillating disk (thin solid line). The accretion rate for the stationary disk is plotted by the thick line. Time is rescaled by the period of oscillations. For reference we plot also the phase of disk oscillations (dotted line) The accretion rate is modulated with twice the frequency of oscillations.

their claim and presented simple arguments why the no torque inner boundary condition is natural if an accretion disk is geometrically thin (Paczynski 2000), but the referee could not be convinced. Thanks to the electronic preprint server, the paper Paczynski (2000) is readily accessible to all interested readers, who can judge its validity.”

A more detailed quantitative analysis of the inner boundary condition, refining arguments given by Paczynski (2000) and making them more precise, was done by Afshordi & Paczynski (2003). They found that Krolik (1999), Gammie (1999), and Agol & Krolik (2000) were qualitatively correct: a classical thin steady-state disk must have some torque at the ISCO, but the effect is not as strong as claimed by Krolik, Gammie and Agol.

Bohdan’s line of argument is as follows:

- Today, the only models that make solid quantitative predictions about the disk spectra that could be compared with observations are the conventional *steady state*, geometrically thin-disk models based on the classical “no-torque” inner boundary condition at the marginally stable orbit at the ISCO.
- It is not known today whether steady-state thin-disk type accretion is possible at all. For serious technical reasons, not even the most sophisticated 3D MHD numerical models of accretion can describe very thin flows, or include radiative cooling.
- Therefore, all arguments today concerning the behavior of the steady-state flows near the ISCO are incomplete. They *all* make simplifying assumptions.

- The most fundamental property of the steady-state flows near the ISCO is that they must necessarily be transonic (with the speed of sound properly defined to include magnetic effects). The sonic point is the *critical point* in the mathematical sense. It is known from the theory of differential equations that certain regularity conditions must be obeyed at a critical point.
- Krolik, Agol and Gammie do not properly consider the regularity conditions at the critical point(s). This is exactly the reason why the stress they calculate at the ISCO is so large. In all models which take a proper care of this important piece of mathematics and calculate solutions which pass the critical points smoothly, the stress at the ISCO is non-zero, but small.

A very important *numerical* work that supports Paczyński's point of view was completed recently by Shafee & al (2008). It describes results of three-dimensional general relativistic magnetohydrodynamical simulations of geometrically thin accretion disk around a non-spinning black hole. The disk has a relative thickness $h/r \sim 0.005 - 0.1$ over the radius range $(2 - 20)GM/c^2$. In steady state, the specific angular momentum profile of the inflowing magnetized gas deviates by less than 2% from that of the standard thin disk model with the zero-inner-torque assumed. In addition, the magnetic torque at ISCO is only $\sim 2\%$ of the inward flux of the angular momentum at that radius. Both results indicate that magnetic coupling across the inner edge is relatively unimportant for geometrically thin disks around non-spinning black holes, which is in accordance with Paczyński's ideas. However, until a mathematically correct *analytic* model describing thin MHD accretion flows near the ISCO becomes available, the controversy is likely to continue.

Acknowledgments. This work was supported mostly by the Polish Ministry of Science grant N203 009 31/1466, and by two smaller travel grants from Princeton and Harvard universities.

References

- Abramowicz, M.A. 1981, Nature 294, 235
 Abramowicz, M.A. 1985, PASJ, 37, 727
 Abramowicz, M.A., Blaes, O.M., Horák, J., Kluźniak, W., Rebusco, P. 2006, Class. Quantum Grav. 23, 1689
 Abramowicz, M.A., Calvani, M., & Nobili, L. 1980, ApJ, 242, 772
 Abramowicz, M.A., Jaroszyński, M., & Sikora, M. 1979, A&A,
 Abramowicz, M.A., Ellis, G.F.R., & Lanza, A. 1990, ApJ, 361, 470
 Abramowicz, M.A., & Piran, T. 1980, ApJ, 241, L7
 Afshordi, N., & Paczynski, B. 2003, ApJ, 592, 354
 Agol, E., & Krolik, J.H. 2000, ApJ, 528, 161
 Blaes, O.M. 1985, MNRAS, 216, 553
 Blaes, O.M. 1987, MNRAS, 227, 975
 Blaes, O.M., Hubeny, I., Algol, E., & Krolik, J.H. 2001, ApJ, 563, 560
 Blanford, R.D., & Znajek, R.L. 1977 MNRAS179, 433
 Czerny, B., & Elvis, M. 1987, ApJ, 321, 305
 Frank, J., King, A.R., & Raine, D.J. 2002, *Accretion Power in Astrophysics*, CUP, Cambridge
 Gammie, C.F. 1999, ApJ, 522, L57

- Igumenshchev, I.V., & Abramowicz, M.A. 2000, ApJS, 130, 463
Jaroszyński, M., Abramowicz, M.A., & Paczyński, B. 1980, Acta Astr., 30, 1
King, A.R. 2002, MNRAS, 335, L13
Komissarov, S.S. 2006, MNRAS, 368, 993
Kozłowski, M., Abramowicz, M.A., & Jaroszyński, M. 1978 A&A, 63, 209
Krolik, J.H. 1999 ApJ, 515, L73
Lynden-Bell, D. 1982, Observatory 102, 131
Madau, P. 1988, ApJ243, 700
Madej, J., & Paczyński, B. 1977, IAU Coll 42, 313 (1977)
Malkan, M. 1989, in *Theory of accretion disks*, eds. F. Meyer & al., Reidel, Dordrecht
Paczynski, B. 1980, seminar at the Copernicus Centre in Warsaw
Paczynski, B. 1982, Astr. Gesellschaft, 57, 27
Paczynski, B. 1998, Acta Astr., 48, 667
Paczynski, B. 1998, preprint., astro-ph-0004129
Paczynski, B., & Wiita, P.J. 1980, A&A, 88, 23-31
Papaloizou, J.C.B., & Pringle, J.E. 1984, MNRAS, 208, 799
Qian, L., Abramowicz, M.A., Fragile C.P., Horák, J., & Machida, M. 2008, A&A, submitted
Rees, M.J., Phinney, E.S., Begelman, M.C., & Blandford, R.D. 1982 Nature, 295, 17
Sikora, M. 1981, MNRAS, 196, 257
Shafee, R., McKinney, J.C., Narayan, R., Tchekhovosky, A., Gammie, C.F, McClintock J.E. 2008, ApJ, submitted
Sikora, M., & Wilson, D.B. 1981 MNRAS, 197, 529
Straub, O., & Šramková, E. 2008, Class. Quantum Grav., submitted